



Optimized Synthesis of FeNi/TiO₂ Green Nanocatalyst for High-Quality Liquid Fuel Production via Mild Pyrolysis

Riny Yolanda Parapat^{1,3,*}, Muhamad Firmansyah Rizkiawan Putra¹, Zamaludin¹, Didin Agustian Permadi², Imam Aschuri³, Yuono¹, Alfian Noviyanto⁴, Michael Schwarze⁵, Reinhard Schomäcker⁵



¹ Chemical Engineering Department, Institut Teknologi Nasional Bandung, PHH. Mustopha 23, 40124 Bandung, Indonesia

² Environmental Engineering Department, Institut Teknologi Nasional Bandung, PHH. Mustopha 23, 40124 Bandung, Indonesia

³ Civil Engineering Department, Institut Teknologi Nasional Bandung, PHH. Mustopha 23, 40124 Bandung, Indonesia

⁴ Nano Center Indonesia, Kawasan Puspitek, Gedung 410 – Ruang B07, Serpong, Indonesia

⁵ Chemistry Department, Technische Universität Berlin, Straße des 17. Juni 124, 10623 Berlin, Germany

* Corresponding author: rinyyolanda@itenas.ac.id

<https://doi.org/10.14710/jksa.26.10.391-403>

Article Info

Article history:

Received: 25th September 2023

Revised: 24th November 2023

Accepted: 27th November 2023

Online: 23rd December 2023

Keywords:

FeNi/TiO₂; mild pyrolysis; nanocatalyst; asphalt; Asbuton; diesel-like oil

Abstract

In sustainable energy improvement, the strategic design of economical nanocatalysts has emerged as a pivotal pathway, notably within intricate processes such as asphalt pyrolysis. This study presents a new endeavor, conceptualizing a non-precious metal nanocatalyst FeNi deposited on TiO₂, synthesized through an environmentally conscious green synthesis methodology employing mangosteen peel extract as a sustainable reductant. Asphalt, the most complex compound, is used as the pyrolyzed material to measure the activity of nanocatalysts in mild pyrolysis. In this study, the synthesis of the nanocatalyst and pyrolysis are optimized. The research outcomes reflect a notable work towards efficiency enhancement. Initial investigations showcased the highest values before optimization for nanocatalyst synthesis, oil yield, and calorific value, which are 63.23%, 50.78%, and 10684 cal/g, respectively. However, these values increase significantly after optimization to 68.44%, 53.72%, and 10775 cal/g, respectively. Careful validation endeavors have underscored the closeness, manifesting slight errors of 2.52%, 1.86%, and 0.36% for catalyst yield, oil yield, and calorific value, respectively. This validation features the reliability of the research findings. Intriguingly, the GC-MS analysis establishes compelling parallels in composition between the derived product and conventional diesel fuel. The minimal errors and the analogous composition to diesel fuel present a promising trajectory. The results obtained from this study contribute to the development of greener and more efficient energy production technologies, paving the way for a sustainable and eco-friendly approach to utilizing energy resources.

1. Introduction

Developing sustainable and environmentally friendly technologies for converting heavy organic materials into valuable products has gained significant attention in recent years [1, 2]. Pyrolysis, a thermochemical process involving the thermal decomposition of organic materials without oxygen, offers a promising pathway for producing liquid fuels, char, and valuable chemicals. However, the conventional

process of asphalt pyrolysis often suffers from limitations, which are typically carried out at high temperatures, more than 500°C [3, 4]. Although asphalt pyrolysis is a long-standing and widely implemented conversion process, there are still areas where improvements can be made. This study explored greener methods for preparing a nanocatalyst, aiming to enhance pyrolysis oil production with high yield and quality.

Nanocatalysts have emerged as a potential strategy to address these challenges and enhance the efficiency and selectivity of asphalt pyrolysis. Among the various catalysts investigated, transition metal-based catalysts, such as FeNi alloy nanoparticles supported on titanium dioxide (FeNi/TiO₂), have shown great promise due to their remarkable catalytic properties and high thermal stability [5, 6]. Using nanocatalysts, such as FeNi, in the pyrolysis process offers several advantages over conventional catalysts like zeolite [7, 8]. Nanocatalysts typically exhibit higher surface area and increased surface-to-volume ratio than conventional catalysts. This unique characteristic provides more active sites for catalytic reactions, resulting in enhanced catalytic activity. FeNi nanoparticles, when supported on a suitable material like TiO₂, can promote the cracking and reforming reactions during pyrolysis, leading to improved conversion rates and higher yields of desired products. Also, nanocatalysts offer the opportunity to control and tailor the selectivity of the pyrolysis process. The small particle size and high dispersion of FeNi nanoparticles on the TiO₂ support can influence the reaction pathways and favor specific reaction products. This selectivity control is particularly crucial in pyrolysis, where the desired product distribution must be optimized for producing biofuels, valuable chemicals, or specific intermediates.

FeNi nanocatalysts can exhibit superior thermal stability than conventional catalysts [9, 10]. The high surface area and well-dispersed nature of nanocatalysts contribute to improved resistance against sintering and agglomeration at high temperatures, ensuring long-term catalytic performance and stability during pyrolysis [11, 12]. Nanoscale dimensions of FeNi nanoparticles allow faster diffusion of reactants and products and efficient heat transfer. This feature facilitates the contact between the catalytic sites and the feedstock, enhancing mass transfer kinetics and improving the overall efficiency of the pyrolysis process. The improved mass and heat transfer characteristics improve conversion rates and reduce energy consumption [13, 14]. The combination of FeNi nanoparticles with a suitable support material, such as TiO₂, can lead to synergistic effects that further enhance the catalytic performance [15, 16].

The presence of FeNi nanoparticles can facilitate the activation of reactant molecules, promote electron transfer, and enhance the adsorption and desorption of intermediates, resulting in improved catalytic efficiency and reaction selectivity [17, 18]. Nanocatalysts offer precise control over their size, shape, and composition during synthesis. This allows researchers to optimize the catalyst's properties for specific pyrolysis applications, tailoring them to the desired reaction conditions, feedstock characteristics, and targeted product distribution [19, 20]. Such flexibility in catalyst design enables the development of efficient and customized catalytic systems for the pyrolysis process. Researchers are still actively focusing on developing green and sustainable synthesis methods for catalyst preparation [21, 22, 23, 24, 25]. Utilizing natural and renewable resources as reducing agents can provide an eco-friendly

alternative to conventional chemical reductants. In this regard, mangosteen peel, a waste product generated by the food industry, has gained attention as a potential green and cost-effective source of reducing agents. Mangosteen peel is known to contain abundant bioactive compounds, including phenolics and antioxidants, which can serve as reducing agents and stabilizers during catalyst synthesis [22, 23].

In this study, we aim to develop a green nanomaterial catalyst, FeNi/TiO₂, to promote the asphaltite pyrolysis processes. Pyrolysis is a thermal method that involves decomposing organic materials into gas, liquid, and solid products without oxygen [26, 27]. FeNi/TiO₂ nanomaterial catalysts in asphaltite pyrolysis aim to enhance reaction efficiency, reduce pyrolysis temperatures, and generate products with improved properties [28, 29]. Here, we also investigated the influence of synthesis parameters of nanocatalyst preparation on the Yield of pyrolysis and the calorific value of pyrolysis products. The results of this research are expected to provide a better understanding of the preparation of nanomaterial catalysts (in this case, FeNi/TiO₂) in asphaltite pyrolysis. With a deeper understanding of the interactions between the catalyst and asphaltite during the pyrolysis process, we can optimize reaction conditions to enhance the desired product yield, reduce the formation of unwanted by-products, and extend the lifespan of asphaltite.

The use of green nanocatalysts in the pyrolysis process holds significant environmental benefits [30, 31]. FeNi/TiO₂ nanomaterial catalysts can reduce the use of hazardous chemicals and mitigate greenhouse gas emissions during asphaltite production [32, 33]. This aligns with global efforts to reduce negative environmental impacts and contribute to sustainable development. This study aims to develop a green nanomaterial catalyst based on FeNi/TiO₂ for use in asphaltite pyrolysis processes. This research is expected to provide new insights into using nanomaterial catalysts in asphaltite pyrolysis and drive the development of more efficient and sustainable technologies in the pyrolysis process. Furthermore, using mangosteen peel as a green reducing agent demonstrates the potential for waste biomaterials for catalyst synthesis, promoting the concept of circular economy and reducing waste generation.

2. Experimental

2.1. Materials

To synthesize FeNi/TiO₂ nanocatalysts, a straightforward method known as the precipitated synthesis approach was employed. Nickel chloride hexahydrate (NiCl₂·6H₂O, 99.9%, Sigma-Aldrich) and iron chloride hexahydrate (FeCl₂·6H₂O, 99.9%, Sigma-Aldrich) served as the metal precursors and were dissolved in deionized water. The reducing solution was prepared by dissolving mangosteen peel (Mastin®, Indonesia), as specified in Table 1, in 100 mL of deionized water. Subsequently, an extraction process was conducted by stirring the mixture at 700 rpm and 70°C for one hour. The extracted solution was then centrifuged to

eliminate solid components efficiently. CristalActiv-TiO₂ (PC-105, Tronox) was utilized as the supporting material for the nanocatalyst. The attached FeNi nanocatalyst on the TiO₂ surface was cleansed using acetone (99.9%, Carl-Roth). As for the pyrolysis process, the asphalt source originated from Asbuton grains supplied by PT. Putindo Bintech, Indonesia.

2.2. Synthesis of FeNi/TiO₂ Nanoparticles

In the first step of synthesizing the nanocatalyst, 25 mg of the mixture solution of Fe and Ni precursors was introduced into the reactor. Subsequently, 25 mg of the reducing solution containing the mangosteen peel extract was added to the reactor using a micro pump with a flow rate of 0.2 mL/s. The thermostat was started, and the temperature was adjusted to 25°C. The stirrer was then set at 700 rpm, initiating the synthesis process. The duration corresponds to the time in Table 1.

Afterward, TiO₂ support was added to the reactor. The mixture was then subjected to a deposition process for 2 hours. The FeNi nanoparticles deposited onto the TiO₂ support were separated using a centrifuge, followed by a thorough wash with pure acetone, and then subjected to a calcination process at 300°C for 2 hours. This procedure was used to prepare the FeNi/TiO₂ nanocatalysts according to Table 1. For the Central Composite Design (CCD) experimental data, the specific design used is presented in Table 2, whereas the factors and levels are shown in Table 3.

Table 1. Factor and level in the synthesis of FeNi/TiO₂ according to 2⁴ FFD

Factor	Level		Description
	Low (-1)	High (+1)	
A FeNi in precursors (mg)	2.564	7.694	The Fe: Ni ratio in the mixture of the precursors FeCl ₂ .4H ₂ O and NiCl ₂ .4H ₂ O is set at 1:3.8. These precursors are combined with water until the total weight reaches 25 mg.
B Natural reductant (mg)	250	390	Amount of mangosteen peel to be extracted (see the procedure in Section 2.1).
C Support (mg)	1450	3900	Amount of TiO ₂ powder to support FeNi nanoparticles
D Time (hr)	1	2	Synthesis time is the time for FeNi nanoparticle formation, excluding the time for deposition.

Table 2. Design summary and point types for the CCD

Design Summary		Point Types	
Factors	4	Cube points	16
Base runs	31	Center points in the cube	7
Base blocks	1	Axial points	8
Replicates	1	Center points in axial	0
Total runs	31	Alpha	1.9
Total blocks	1		

Table 3. Factor and level in the synthesis of FeNi/TiO₂ according to CCD

Factor	Level				
	-1.9	-1	0	1	1.9
A FeNi in precursors (mg)	0.255	2.564	5.129	7.694	10.002
B Natural reductant (mg)	191.95	250	314.50	390	437.05
C Support (mg)	347.5	1450	2675	3900	5002
D Time (hr)	0.55	1	1.5	2	2.45

2.3. Pyrolysis of Asphalt

The pyrolysis setup is depicted in Figure 1. Before starting the pyrolysis process, a preliminary step involved reducing the size of 50 g of Asbuton through ultrasonic treatment in the presence of an acetone solvent for 35 minutes. Subsequently, the Asbuton, now finely dispersed within the acetone, is introduced into the reactor alongside the catalyst. Following this initial setup, the reactor heater is configured to maintain a temperature of 70°C, effectively separating the acetone from the feed material.

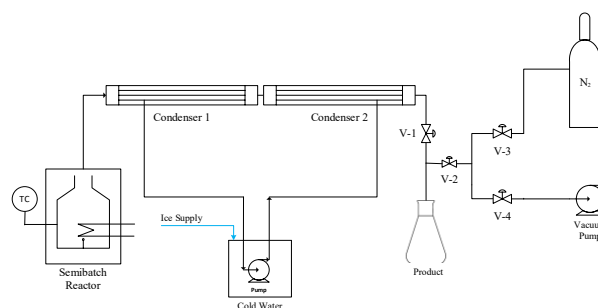


Figure 1. Schematic of the pyrolysis process

The evaporated acetone is then channeled through a condenser, which undergoes condensation and is collected in an Erlenmeyer flask. The condensed acetone is subsequently transferred to a separate container. The Erlenmeyer flask is then reconnected to the condenser, and a vacuum pump is activated to evacuate any residual

air within the reactor. This step introduces nitrogen to manage a reactor pressure of 1 atm, replacing the air. Subsequently, the temperature is elevated to 400°C, initiating the pyrolysis process, which continues for 3 hours, yielding valuable pyrolysis oil products.

3. Results and Discussion

3.1. Full Factorial Design with Three Responses

The first attempt of experiments was using 2⁴ Full Factorial Design with three responses, as shown in Table 2. The appearances of collected pyrolysis oil are presented in Figure 2 correspondingly, showing yellow-transparent in color. In our work, we avoid the presence of O₂ in the system.

Pyrolysis carried out in the presence of O₂ in the system will produce products with a color that tends to be dark or black [34, 35]. The dark color indicates that the resulting oil still has long carbon chains and indirectly suggests that the hydrocarbon chain cracking process is incomplete. The O₂ gas can interfere with the process of cracking the hydrocarbon chain and produce CO₂. To ensure that there is no O₂ gas in the system, inert gas in N₂ is introduced into the system. We conducted the study on mild pyrolysis of bitumen at 400°C to inhibit coke formation, as reported by Zachariah *et al.* [36]. The

addition of light material as a solvent in our work can also suppress coke formation, as they also confirmed.

The calorific values of the samples were tested using the ASTM D4809. The results show that the average calorific value of the samples is 9973 cal/g, with the highest value being 10185 cal/g. These values closely approximate the calorific value of diesel fuel, which falls within the range of 10546 to 10723 cal/g [37]. This value may vary slightly depending on the quality and specific composition of the oil. Therefore, we assume that our transparent product is diesel-like oil because its calorific value closely approaching that of diesel fuel.



Figure 2. Product of asphalt pyrolysis

Table 4. The results based on 2⁴ full factorial design

Run	Factor				Response		
	A	B	C	D	Nanocatalyst Yield (%)	Oil Yield (%)	Calorific Value (Cal/g)
1	-1	-1	-1	-1	62.21	30.70	10070
2	1	-1	-1	-1	49.86	39.15	10185
3	-1	1	-1	-1	79.15	48.60	10006
4	1	1	-1	-1	61.61	31.83	10062
5	-1	-1	1	-1	73.23	46.10	10162
6	1	-1	1	-1	63.91	28.32	9486
7	-1	1	1	-1	57.61	38.75	10095
8	1	1	1	-1	65.04	49.96	10027
9	-1	-1	-1	1	62.03	30.54	9992
10	1	-1	-1	1	69.86	37.20	10684
11	-1	1	-1	1	59.28	44.77	9763
12	1	1	-1	1	63.47	38.47	9972
13	-1	-1	1	1	53.67	50.78	10015
14	1	-1	1	1	68.62	28.16	9685
15	-1	1	1	1	58.92	49.43	9576
16	1	1	1	1	68.82	22.57	9789

In this study, we focus more on the yield and calorific value of pyrolysis oil; however, we later optimize the synthesis yield of FeNi/TiO₂. Figure 3 presents a distinct interaction (generated using Minitab®) among the variations in the composition of FeNi metal, reduction amount, TiO₂ support, and reaction time. It can be inferred from Figure 3 that specific compositions of each factor significantly influence the enhancement of both yield and calorific value of pyrolysis oil. It can be seen that the amount of FeNi has stronger interactions either with TiO₂ support or with synthesis time, in influencing both the Yield and calorific value of oil. This indicates that the impact of the amount of FeNi precursor on the yield and calorific value of pyrolysis oil depends on how much TiO₂ support and synthesis time are used.

To evaluate the level of influence of the factors involved in the pyrolysis process, we use the normal plots of standardized effect, as depicted in Figure 4. It can be seen that the factor that has the most significant effect on the yield of oil is the amount of FeNi in the precursor (A). The quantity of metal catalysts in a nanoscale can significantly influence its catalytic activity [38]. An increased amount of FeNi within the catalyst translates to more active sites available to facilitate the pyrolysis reaction. Consequently, this increased availability of active sites can improve the reaction rate, ultimately leading to an enhanced oil production yield. The quantity of FeNi incorporated into the catalyst can also play a pivotal role in determining its thermal stability [39].

Catalysts containing higher levels of FeNi may possess greater thermal stability, signifying their ability to maintain catalytic activity even under the elevated temperatures requisite for the asphalt pyrolysis process. In other words, by increasing the concentration of FeNi in the nanocatalyst synthesis, the available surface area for interaction with asphalt is correspondingly expanded. This increase enhances the probability of pyrolysis reactions taking place on the catalyst's active sites, thereby contributing to an increased oil yield.

Conversely, catalysts with lower FeNi concentrations may exhibit reduced stability and could undergo deactivation when subjected to high temperatures. In addition to the FeNi content, the particle size of the nanocatalyst can have a bearing on the outcomes of the pyrolysis reaction. Smaller nanoscale particles offer a larger surface area than their larger counterparts. Consequently, nanocatalyst particles with higher FeNi concentrations may exhibit smaller particle sizes, resulting in an enhanced efficiency of the pyrolysis reaction.

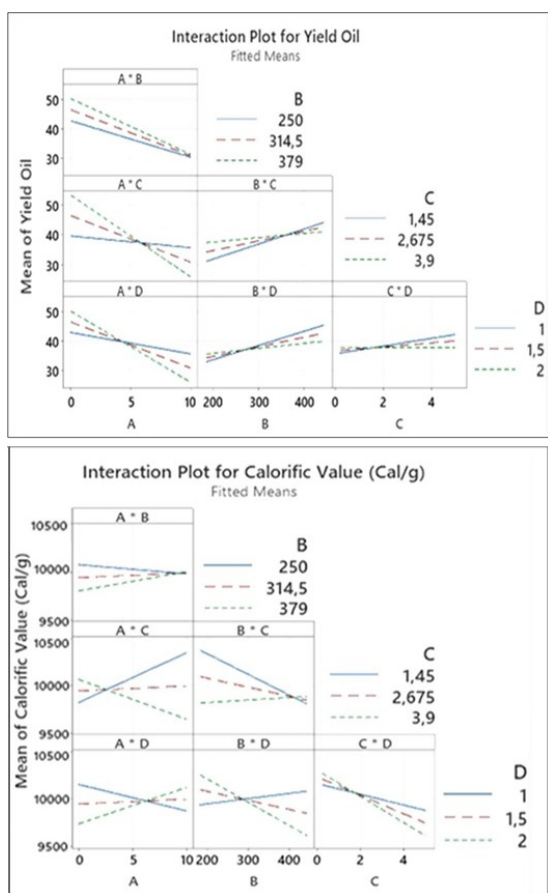


Figure 3. Factor interaction plots for the response of yield (top) and calorific value (bottom) of pyrolysis oil

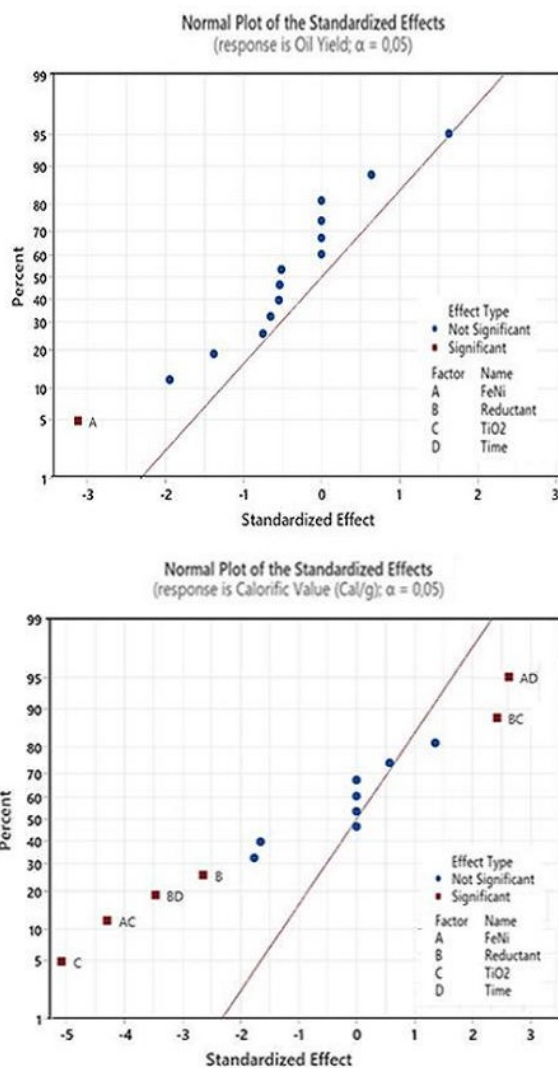


Figure 4 Normal plots of standardized effect for yield (top) and calorific value (bottom) of pyrolysis oil

Figure 4 (bottom) shows that the amount of both TiO₂ support (C) and the natural reductant (B) in the preparation of nanocatalyst affects the calorific value of pyrolysis oil. As a support catalyst, TiO₂ promotes the nanoparticle distribution on its surface, thus impacting the rate of the asphaltene pyrolysis reaction. Subsequently, it is altering the composition of the resulting pyrolysis products. This, in turn, can lead to variations in the calorific value of the pyrolysis oil due to differences in product composition. The influence of natural reducing agents present in mangosteen peel extract during the synthesis of FeNi/TiO₂ nanocatalysts can affect the catalytic properties of the nanocatalyst. Fluctuations in the quantity of these natural reducing

agents can change the physical and chemical characteristics of the nanocatalyst [23, 40], consequently impacting its activity in asphalt pyrolysis. This, in turn, can also influence the composition of the pyrolysis products and, therefore, the calorific value of the resulting oil.

3.2. Optimization of Pyrolysis Process

The comprehensive data for optimizing the pyrolysis process using the central composite design method is presented in Table 3. We use the procedure published by Parapat *et al.* [22] for the optimization. We note here that there were no replications for the variations.

Table 5. Experiment results based on central composite design

Run	Factor				Response		
	(A)	(B)	(C)	(D)	Calorific Value (Cal/g)	Yield of Oil (%)	Yield of Catalyst (%)
1	5.129	314.50	5.003	1.50	9747	40.03	63.92
2	2.564	250.00	3.900	1.00	10162	46.11	73.25
3	0.256	314.50	2.675	1.50	9948	46.08	63.03
4	5.129	314.50	2.675	1.50	9973	38.46	63.61
5	5.129	314.50	2.675	1.50	9973	38.46	63.61
6	2.564	379.00	3.900	1.00	10095	38.78	57.64
7	7.694	379.00	1.450	1.00	10062	31.81	61.61
8	2.564	250.00	3.900	2.00	10015	50.82	53.75
9	7.694	250.00	3.900	2.00	9685	28.17	68.68
10	2.564	379.00	1.450	2.00	9763	44.76	59.32
11	2.564	379.00	3.900	2.00	9575	49.51	59.02
12	5.129	314.50	2.675	1.50	9973	38.46	63.61
13	2.564	250.00	1.450	1.00	10070	30.69	62.23
14	7.694	379.00	3.900	1.00	10027	49.97	65.04
15	5.129	314.50	2.675	1.50	9973	38.46	63.61
16	5.129	314.50	2.675	1.50	9973	38.46	63.61
17	5.129	437.05	2.675	1.50	9855	42.45	64.86
18	2.564	379.00	1.450	1.00	10006	48.59	79.16
19	5.129	314.50	2.675	1.50	9973	38.46	63.61
20	5.129	191.95	2.675	1.50	10090	34.48	62.36
21	5.129	314.50	0.348	1.50	10199	36.90	63.31
22	7.694	379.00	3.900	2.00	9789	22.62	68.90
23	2.564	250.00	1.450	2.00	9992	30.53	62.07
24	7.694	250.00	3.900	1.00	9486	28.31	63.91
25	5.129	314.50	2.675	1.50	9973	38.46	63.61
26	5.129	314.50	2.675	2.45	9900	37.11	62.71
27	7.694	379.00	1.450	2.00	9972	38.45	63.49
28	7.694	250.00	1.450	2.00	10684	37.17	69.89
29	7.694	250.00	1.450	1.00	10185	39.12	49.86
30	10.003	314.50	2.675	1.50	9998	30.84	64.20
31	5.129	314.50	2.675	0.55	10046	39.81	64.51

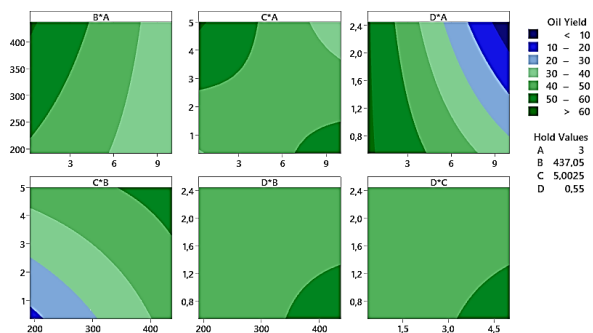


Figure 5. Contour plot of oil yield in the pyrolysis process

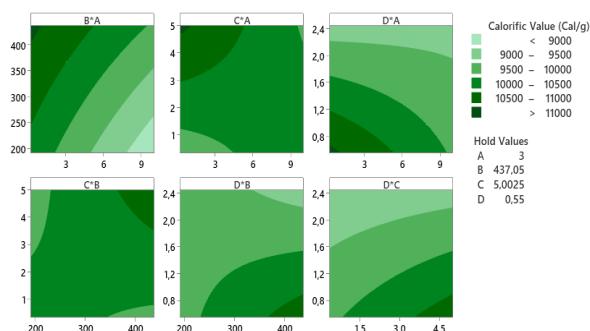


Figure 6. Contour plot of calorific value in the pyrolysis process

In this study, we elaborate on the findings to provide a deeper understanding of the underlying mechanisms governing the pyrolysis process and underscore the significance of catalyst composition and design in achieving sustainable and efficient conversion of asphalt into high-quality liquid fuel. Figures 5 and 6 are the contour plots of yield and calorific value of the pyrolysis oil, illustrating the intricate interaction between the amount of FeNi precursor (A), reducing agent (B), TiO₂ support (C), and the synthesis time, which influences the pyrolysis results. The contour plots depict the connection between each factor that can help with the optimization process. For example, a shorter synthesis time of nanocatalyst (D) leads to a higher yield and calorific value of oil.

Meanwhile, when the amount of mangosteen (B) is around 400 mg or more, the resulting yield and calorific value also attain high levels. It can also be indicated from the contour plot diagram that the calorific values surpassing 10500 can be reached when we prepared the nanocatalyst with the values of FeNi metal, mangosteen peel, TiO₂ support, and reaction time as < 5, > 400, > 5, and < 0.8, respectively. Thus, it can be reasonably concluded that these specific variations possess exceptional prospects for further validation and evaluation. The finding of the maximum response area substantiates their pivotal role in achieving optimal outcomes.

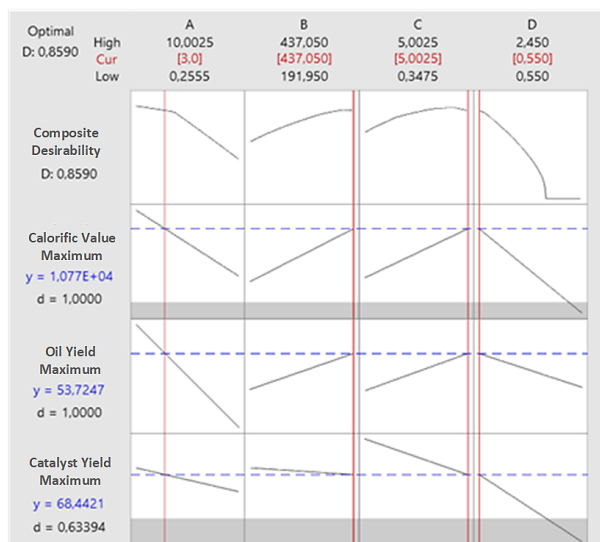


Figure 7. Results of multiple optimizations that simultaneously optimize the oil yield, calorific value, and nanocatalyst yield

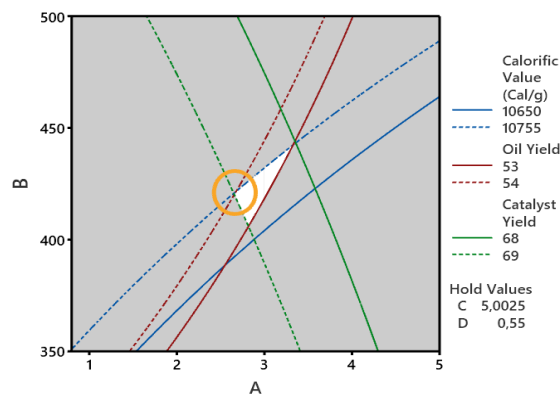


Figure 8. Overlapping contour plots of oil yield, calorific value, and nanocatalyst yield, which results in the optimization point

Figure 7 shows the result of the optimization of the nanocatalyst for a good pyrolysis process. Theoretically, when using FeNi metal salt of 3.0 mg, reducing the amount of 437.05 mg, TiO₂ support of 5.00 g, and reaction time of 0.55 hr, we can maximize the nanocatalyst yield to 68.44% and also can increase the yield and calorific value of pyrolysis oil to 53.72% and 1077 cal/g, respectively. The optimization results are confirmed by Figure 8, which shows the graphical representation that indicates overlapping intersections among these compositions. The validation aligns precisely with the optimization values found in Figure 7. We conduct an experiment using the corresponding values to validate the theoretical optimization results. Careful validation endeavors have underscored the closeness, manifesting slight errors of 2.52%, 1.86%, and 0.36% for catalyst yield, oil yield, and calorific value, respectively.

3.3. Role of Mangosteen Peel in the Green Synthesis Process of Nanoparticles in Producing Highly Active FeNi Nanocatalysts for Pyrolysis Process

This study aims not only to achieve a high yield and quality of pyrolysis oil at a mild temperature (450°C) but also to highlight a more environmentally friendly (greener) process in terms of catalyst preparation. This involves the utilization of mangosteen peel extract in the nanocatalyst synthesis at room temperature. It has been reported by Parapat *et al.* [22] that mangosteen peel contains a phenolic compound, namely α -mangosteen, serving as the reducing agent in the mangosteen peel extract. This antioxidant plays a crucial role in the formation of nanoparticles. The characterization of mangosteen peel with Infrared (IR) analysis reveals the presence of expected bioactive agents of phenolic compounds through IR spectra, as depicted in Figure 9.

Phenolic compounds consist of one or more aromatic rings, and hydroxyl functions are directly linked to the rings. In the broad O-H stretching vibration bands at wave numbers 3550 to 3230 cm^{-1} , the breadth is caused by interference of hydrogen bonding interactions. The C-H stretching vibration bands are also shown at 2950 – 2850 cm^{-1} . The IR spectra show the bands typical for aromatic compounds in the region of 1500–1600 cm^{-1} . The stretching of the C–H and C=C–C aromatic bond appears in the region of 1615–1580 cm^{-1} . In addition, the phenolic C–O stretching was observed at about 1200 cm^{-1} . The region ranging from 1400 to 900 cm^{-1} is commonly called the fingerprint region because of the large amount of characteristic single bands of low intensities attributed to specific functional groups. The NMR analysis also shows the peaks of hydroxyl functions at 13 ppm and 4.7 ppm, which can be seen in Figure 10.

Before synthesizing, we extracted the mangosteen peel using water as the solvent at 70°C for 30 minutes. With this mild extraction, the major bioactive substance (α -mangosteen) would be extracted [22]. Based on the reduction mechanisms of metal using antioxidants [41], the scheme of Fe^{2+} and Ni^{2+} reduction mechanism by α -mangosteen is displayed in Figure 11. In synthesizing metal nanoparticles, controlling the size and shape of metal particles is crucial. Despite successful attempts by many scientists in synthesizing metal nanoparticles, the resulting shapes predominantly exhibit low-index structures such as (111) and (100). These low-index planes consist of densely packed atoms with fewer edges, kinks, steps, and corners, resulting in low surface energy. Preferably, shapes with high-index planes are desired

due to their higher surface energies, leading to increased activity.

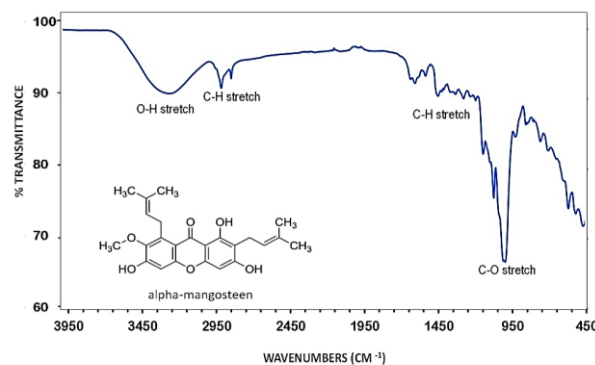


Figure 9. Characterization of mangosteen peel with Infrared (IR) analysis

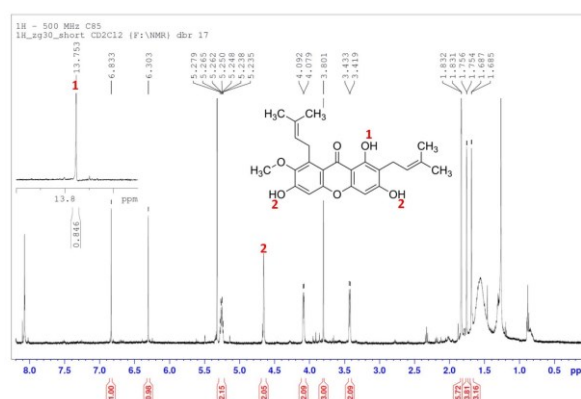


Figure 10. NMR analysis of the mangosteen peel

In general, metal ions reduced by a strong reductant produce nanoparticles with fewer active sites than those reduced by a weak reductant [23, 40]. This is attributed to the slow growth of nanoparticles induced by weak reductants, resulting in the formation of anisotropic nanoparticles. This can be observed in the SEM images in Figure 12 A (inset), which shows the anisotropic (non-symmetrical) shape of the FeNi nanoparticle. Phenolic compounds found in mangosteen peel are categorized as weak reductants, effectively restraining the nucleation and growth processes. Based on our previous work, parameters such as the quantity of metal, reducing agent, support, and synthesis time influence the size and shape of the produced nanoparticles. These parameters dictate the number of atoms located at bends and edges, consequently shaping the surface chemistry. Therefore, optimizing these parameters is essential as they determine the catalytic performance of the nanoparticles.

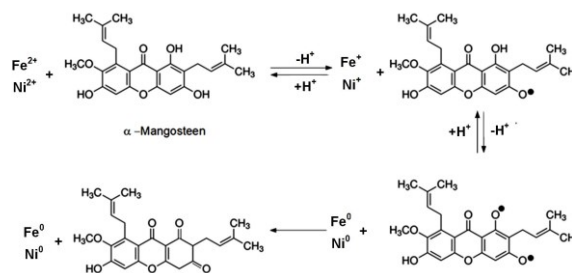


Figure 11. Scheme of Fe^{2+} and Ni^{2+} reduction mechanism by α -mangosteen

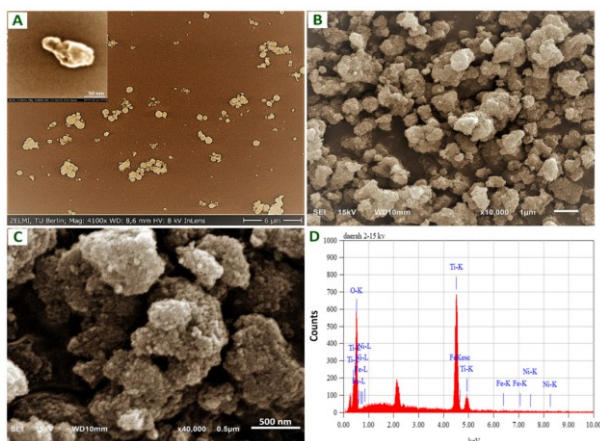


Figure 12. SEM images of (A) FeNi nanoparticles, (B, C) FeNi/TiO₂ nanocatalyst with different magnifications, and (D) the EDS analysis

3.4. Comparison Between the Produced FeNi/TiO₂ Nanocatalysts and Other Catalysts in Asphalt Pyrolysis

This study also tested some other catalysts in Asbuton pyrolysis using our reactor and compare their performances with our FeNi/TiO₂ nanocatalysts. As shown in Figure 14, the optimized FeNi/TiO₂ produced in this work has the largest oil yield compared to SiO₂, AlSi, Al₂O₃, synthetic Zeolite, and natural Zeolite. These findings indicate that FeNi/TiO₂ nanocatalysts exhibit a higher catalytic activity level in the asphalt pyrolysis process than other catalysts.

As previously mentioned, the FeNi nanocatalyst produced in this work exhibits an anisotropic (non-symmetrical) shape. This distinctive characteristic significantly contributes to the enhanced activity of the resulting FeNi nanocatalyst, leading to a superior product compared to other catalysts. This is attributed to the absence of nanoparticles in those reduced catalysts using bioactive substances as the reducing agents. In addition, the high yield of the produced pyrolysis oil is also due to the nanoscale of FeNi nanoparticles that are well distributed on TiO₂ support, as seen in SEM images of FeNi/TiO₂ (Figure 12 B and C). The presence of Fe and Ni on TiO₂ is confirmed through EDS analysis (Figure 12 D). The average size of FeNi nanoparticles is determined using the Scherrer equation based on XRD data measurements, as illustrated in Figure 13, yielding a diameter of 13 nm.

This improved catalytic activity has the potential to accelerate pyrolysis reactions, consequently leading to elevated oil yields. FeNi/TiO₂ nanocatalysts may boast superior surface characteristics, including improved surface area and increased catalytic sites. This increase can significantly enhance the efficiency of the pyrolysis reaction by providing an abundance of active sites available to interact with the Asbuton, thereby yielding a greater quantity of oil. Also, the thermal stability of FeNi/TiO₂ nanocatalyst may surpass that of other catalysts such as zeolite or Al₂O₃. This heightened thermal stability ensures that the catalyst remains active even under the elevated temperatures necessitated by the pyrolysis of Asbuton, preventing deactivation.

The utilization of natural reducing agents derived from mangosteen peel extract during the synthesis of nanocatalysts can significantly impact the anisotropic shape of the produced FeNi. Compounds present in mangosteen peel extract may possess properties conducive to favoring the pyrolysis reaction or engaging in positive interactions with the catalyst, thereby enhancing its overall performance. The synergy between FeNi/TiO₂ and naturally reducing mangosteen peel extract could result in a distinctive combination of properties, which synergistically support the Asbuton pyrolysis reaction, ultimately leading to remarkably high oil yields.

Another advantage is that utilizing FeNi nanocatalysts with natural reducing agents embraces an environmentally friendly approach by utilizing reusable mangosteen rind as the reducing agent. From an economic perspective, employing FeNi nanocatalysts with natural mangosteen reduction offers advantages due to the wide availability of materials such as FeNi and mangosteen peel, leading to more affordable pricing. The accessibility of these economically viable products promotes the preference for these nanocatalysts in the pyrolysis process, thus contributing to environmental benefits. This research opens new possibilities for developing sustainable pyrolysis processes and significantly contributes to the prudent management of natural resources.

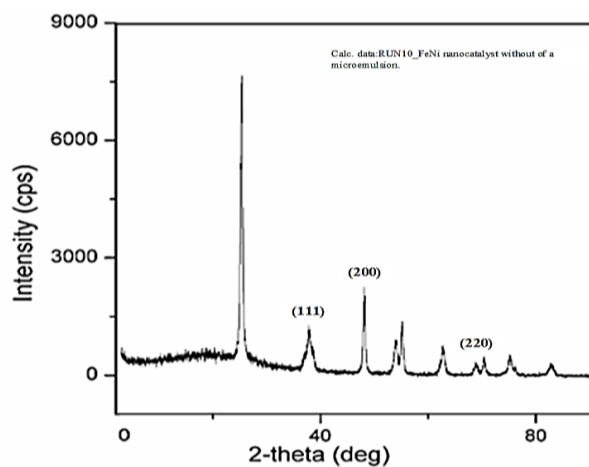


Figure 13. XRD of FeNi/TiO₂ nanocatalyst

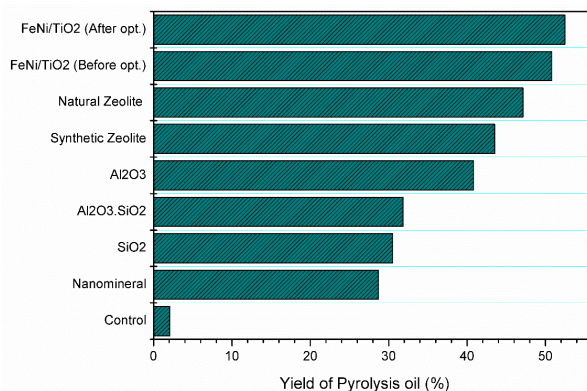


Figure 14. Oil yield comparison between FeNi/TiO₂ nanocatalysts and various other catalysts in pyrolysis outcomes

Table 6. GCMS analysis results

Peak Nr	Retention Time	Compound Name	Compound Formula	Area (%)	Height	Height (%)
1	12.223	Benzene, 1-ethyl-2-methyl-	C ₉ H ₁₂	1.89	8404018	2.21
2	12.260	Benzene, 1,3,5-trimethyl- (CAS) 1,3,5-Trimethylbenz	C ₉ H ₁₂	0.54	6669935	1.75
3	12.819	Benzene, 1-ethyl-3-methyl-	C ₉ H ₁₂	0.85	5740954	1.51
4	13.338	Benzene, 1,2,3-trimethyl- (CAS) 1,2,3-Trimethylbenz	C ₉ H ₁₂	3.38	15294563	4.02
5	13.498	Decane (CAS) n-Decane	C ₁₀ H ₂₂	0.67	5070812	1.33
6	14.245	Benzene, 1,2,4-trimethyl- (CAS) 1,2,4-Trimethylbenz	C ₉ H ₁₂	1.04	7275726	1.91
7	16.733	Undecane	C ₁₁ H ₂₄	0.94	7114193	1.87
8	19.780	Dodecane (CAS) n-Dodecane	C ₁₂ H ₂₆	1.56	10029786	2.64
9	22.633	Tridecane (CAS) n-Tridecane	C ₁₃ H ₂₈	2.64	12236534	3.22
10	23.041	Naphthalene, 1-methyl- (CAS) 1- Methylnaphthalene	C ₁₁ H ₁₀	0.59	3153136	0.83
11	24.651	Dodecane, 2,7,10-trimethyl-	C ₁₅ H ₃₂	0.53	4179427	1.10
12	25.310	Tetradecane (CAS) n-Tetradecane	C ₁₄ H ₃₀	2.43	13763138	3.62
13	25.535	Naphthalene, 1,7-dimethyl- (CAS) 1,7-Dimethylnaph	C ₁₂ H ₁₂	0.72	3169588	0.83
14	25.937	Naphthalene, 1,2-dimethyl- (CAS) 1,2-Dimethyl Naphthalene	C ₁₂ H ₁₂	0.97	4122382	1.08
15	26.020	Naphthalene, 2,6-dimethyl- (CAS) 2,6-Dimethylnaphthalene	C ₁₂ H ₁₂	0.46	3135282	0.82
16	26.832	Undecane, 3,8-dimethyl- (CAS)	C ₁₃ H ₂₈	1.49	6210416	1.63
17	27.816	Pentadecane (CAS) n-Pentadecane	C ₁₅ H ₃₂	3.03	16177086	4.25
18	29.053	Hexadecane, 7,9-dimethyl-	C ₁₈ H ₃₈	0.58	2372869	0.62
19	30.176	Hexadecane	C ₁₆ H ₃₄	2.84	16050953	4.22
20	31.238	Pentadecane, 2,6,10-trimethyl-	C ₁₈ H ₃₈	0.74	4490026	1.18
21	32.413	Heptadecane	C ₁₇ H ₃₈	2.82	14423930	3.79
22	32.531	Pentadecane, 2,6,10,14- tetramethyl-	C ₁₉ H ₄₀	2.56	12976947	3.41
23	32.984	Tetradecanoic acid, methyl ester (CAS), Methyl myristate	C ₁₅ H ₃₀	0.65	4772681	1.25
24	34.533	Iron, tricarbonyl[N-(phenyl-2- pyridinyl methylene)benzenamine- N,N']-	C ₃₁ H ₁₄ FeN ₂ O ₃	2.40	13545753	3.56
25	34.690	Hexadecane, 2,6,10,14-tetramethyl- (CAS) Phytane	C ₂₀ H ₄₂	0.76	4378505	1.15
26	36.553	Nonadecane (CAS) n-Nonadecane	C ₁₉ H ₄₀	2.24	10563690	2.78
27	37.338	Hexadecanoic acid, methyl ester (CAS), Methyl palmitate	C ₁₇ H ₃₄ O ₂	21.08	33093345	8.70
28	38.494	Eicosane (CAS) n-Eicosane	C ₂₀ H ₄₂	2.07	12093656	3.18
29	40.345	9,12-Octadecadienoic acid (Z, Z)-, methyl ester (CAS) Methyl linoleate	C ₁₉ H ₃₄ O ₂	2.33	9450117	2.48
30	40.647	9-Octadecenoic acid, methyl ester (CAS) Methyl Octadec-9-Enoate	C ₁₉ H ₃₆ O ₂	24.43	34035524	8.94
31	40.948	Octadecanoic acid, methyl ester (CAS) Methyl stearate	C ₁₉ H ₃₈ O ₂	3.30	17380485	4.57
32	42.069	Docosane (CAS) n-Docosane	C ₂₂ H ₄₆	1.71	11149906	2.93
33	43.488	Nonacosane (CAS) n-Nonacosane	C ₂₉ H ₆₀	1.51	11625273	3.05
34	44.683	Heneicosane	C ₂₁ H ₄₄	1.29	10397647	2.73
35	45.726	Pentacosane (CAS) n-Pentacosane	C ₂₅ H ₅₂	1.05	9203154	2.42
36	46.660	Hexacosane (CAS) n-Hexacosane	C ₂₆ H ₅₄	0.83	7574826	1.99
37	47.516	Tetratetracontan	C ₄₄ H ₉₀	0.62	5815824	1.53
38	48.804	Cyclopropanecarboxylic acid, 3- (2,2-dichloroethenyl)-2,2- dimethyl-, cyano(3- phenoxyphenyl)methyl ester	C ₂₂ H ₁₉ Cl ₂ NO ₃	0.48	3427933	0.90

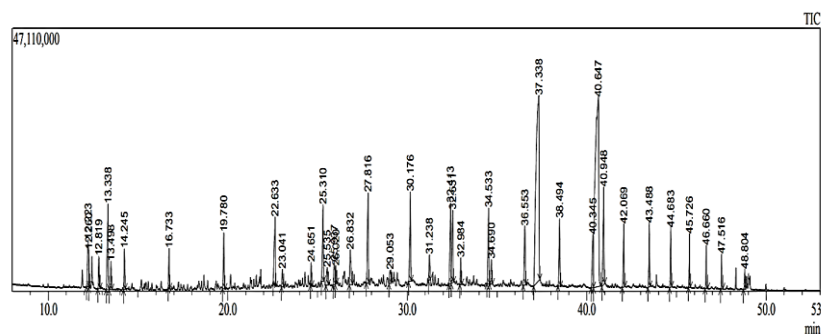


Figure 15. Chromatogram of GCMS analysis results

Based on the research findings, our process effectively achieved a calorific value closely resembling diesel fuel, yielding a test result of 10716 cal/g. To ensure the product quality of the optimized results, we proceeded with comprehensive testing of our products using GCMS analysis (Table 6 and Figure 15). The GCMS results demonstrated the excellent quality of the pyrolysis oil, closely aligning with the GCMS results from diesel fuel. The good quality of the produced pyrolysis oil is attributed again to the small size and anisotropic shape of FeNi nanoparticles that are well distributed on TiO₂ support.

4. Conclusion

The assembly of green FeNi/TiO₂ using CCD optimization techniques for mild pyrolysis of asphalt has been demonstrated. The research results illustrate the influence of the factors used in nanocatalyst preparation on the quantity and quality of pyrolysis oil. The designed nanocatalysts exhibited remarkable catalytic activity, leading to significantly improved yields in the asphalt pyrolysis process. Notably, the high catalytic activity of the FeNi-TiO₂ nanocatalyst was achieved by utilizing a natural reducing agent, mangosteen peel extract. This eco-friendly synthesis approach not only enhances the effectiveness of the process but also aligns with environmental sustainability. Furthermore, the resulting pyrolysis products were found to possess calorific values closely resembling diesel fuel, further substantiated through GC-MS analysis. The synthesis parameters required to achieve the desired optimal results are as follows: 3 mg FeNi (with a ratio of 1:3.8) in the precursor solution, 437.05 mg of mangosteen peel to be extracted, 5.00 g of TiO₂ support to deposit the produced nanoparticles and a synthesis time of 0.55 hr. The attained optimal outcomes consist of an oil yield of 53.72%, a heating value of 10775 cal/g (equivalent to the calorific value of diesel oil), and a catalyst yield of 68.44%. Remarkably, when employing the FeNi/TiO₂ nanocatalyst prepared through the green process with mangosteen peel, the resulting oil yield surpasses previously employed catalysts. This research offers a promising solution for enhancing heavy organic pyrolysis processes and contributes to developing sustainable energy resources.

Acknowledgment

The authors are grateful to the Ministry of Technology Research and Higher Education (Ristekdikti)

of Indonesia for the financial support. Special thanks to Muhammad Nadhif Noer Hamdhan and Daniel Christian Brüggemann for helping us in NMR analysis.

References

- [1] Rick Arneil D. Arancon, Carol Sze Ki Lin, King Ming Chan, Tsz Him Kwan, Rafael Luque, Advances on waste valorization: new horizons for a more sustainable society, *Energy Science & Engineering*, 1, 2, (2013), 53-71 <https://doi.org/10.1002/ese.3.9>
- [2] Mingyuan He, Yuhan Sun, Buxing Han, Green Carbon Science: Efficient Carbon Resource Processing, Utilization, and Recycling towards Carbon Neutrality, *Angewandte Chemie International Edition*, 61, 15, (2022), e202112835 <https://doi.org/10.1002/anie.202112835>
- [3] Ahmed M. Elgarahy, Ahmed Hammad, Dina M. El-Sherif, Mohamed Abouzid, Mohamed S. Gaballah, Khalid Z. Elwakeel, Thermochemical conversion strategies of biomass to biofuels, techno-economic and bibliometric analysis: A conceptual review, *Journal of Environmental Chemical Engineering*, 9, 6, (2021), 106503 <https://doi.org/10.1016/j.jece.2021.106503>
- [4] Gong Jing-Song, Fu Wei-Biao, Zhong Bei-Jing, A study on the pyrolysis of asphalt, *Fuel*, 82, 1, (2003), 49-52 [https://doi.org/10.1016/S0016-2361\(02\)00136-9](https://doi.org/10.1016/S0016-2361(02)00136-9)
- [5] Zeyu Bian, Shihan Dai, Liang Wu, Zhe Chen, Mingliang Wang, Dong Chen, Haowei Wang, Thermal stability of Al-Fe-Ni alloy at high temperatures, *Journal of Materials Research and Technology*, 8, 3, (2019), 2538-2548 <https://doi.org/10.1016/j.jmrt.2019.01.028>
- [6] Ningning Liang, Runrun Xu, Guanzhong Wu, Xuzhou Gao, Yonghao Zhao, High thermal stability of nanocrystalline FeNi₂CoMo_{0.2}V_{0.5} high-entropy alloy by twin boundary and sluggish diffusion, *Materials Science and Engineering: A*, 848, (2022), 143399
- [7] Maryum Ali, Erum Pervaiz, Tayyaba Noor, Osama Rabi, Rubab Zahra, Minghui Yang, Recent advancements in MOF-based catalysts for applications in electrochemical and photoelectrochemical water splitting: A review, *International Journal of Energy Research*, 45, 2, (2021), 1190-1226 <https://doi.org/10.1002/er.5807>
- [8] Dingding Yao, Chi-Hwa Wang, Pyrolysis and in-line catalytic decomposition of polypropylene to carbon nanomaterials and hydrogen over Fe- and Ni-based catalysts, *Applied Energy*, 265, (2020), 114819 <https://doi.org/10.1016/j.apenergy.2020.114819>

- [9] Shifei Kang, Maofen He, Chaochuang Yin, Haiyang Xu, Qing Cai, Yangang Wang, Lifeng Cui, Graphitic carbon embedded with Fe/Ni nano-catalysts derived from bacterial precursor for efficient toluene cracking, *Green Chemistry*, 22, 6, (2020), 1934–1943 <https://doi.org/10.1039/C9GC03357B>
- [10] Qiming Sun, Ning Wang, Qiming Bing, Rui Si, Jingyao Liu, Risheng Bai, Peng Zhang, Mingjun Jia, Jihong Yu, Subnanometric Hybrid Pd-M(OH)₂, M = Ni, Co, Clusters in Zeolites as Highly Efficient Nanocatalysts for Hydrogen Generation, *Chem*, 3, 3, (2017), 477–493 <https://doi.org/10.1016/j.chempr.2017.07.001>
- [11] Yumei Peng, Yiwen Zhang, An Guo, Mingyue Mao, Yi Wang, Yan Long, Guangyin Fan, Universal low-temperature oxidative thermal redispersion strategy for green and sustainable fabrication of oxygen-rich carbons anchored metal nanoparticles for hydrogen evolution reactions, *Chemical Engineering Journal*, 433, (2022), 133648 <https://doi.org/10.1016/j.cej.2021.133648>
- [12] Haifeng Xiong, Abhaya K. Datye, Yong Wang, Thermally Stable Single-Atom Heterogeneous Catalysts, *Advanced Materials*, 33, 50, (2021), 2004319 <https://doi.org/10.1002/adma.202004319>
- [13] R. Kumar, V. Strezov, H. Weldekidan, J. He, S. Singh, T. Kan, B. Dastjerdi, Lignocellulose biomass pyrolysis for bio-oil production: A review of biomass pre-treatment methods for production of drop-in fuels, *Renewable and Sustainable Energy Reviews*, 123, (2020), 109763 <https://doi.org/10.1016/j.rser.2020.109763>
- [14] Abhishek Sharma, Vishnu Pareek, Dongke Zhang, Biomass pyrolysis—A review of modelling, process parameters and catalytic studies, *Renewable and Sustainable Energy Reviews*, 50, (2015), 1081–1096 <https://doi.org/10.1016/j.rser.2015.04.193>
- [15] Xiaocong Gu, Zong Liu, Meng Li, Jingqi Tian, Ligang Feng, Surface structure regulation and evaluation of FeNi-based nanoparticles for oxygen evolution reaction, *Applied Catalysis B: Environmental*, 297, (2021), 120462 <https://doi.org/10.1016/j.apcatb.2021.120462>
- [16] Xin Wu, Lei He, Xiaoyang Wang, Enhanced oxygen evolution reaction performance of synergistic effect of TiO₂/Ti₃C₂/FeNi LDH, *Ceramics International*, 47, 18, (2021), 25755–25762 <https://doi.org/10.1016/j.ceramint.2021.05.302>
- [17] Runze Li, Dingsheng Wang, Superiority of Dual-Atom Catalysts in Electrocatalysis: One Step Further Than Single-Atom Catalysts, *Advanced Energy Materials*, 12, 9, (2022), 2103564 <https://doi.org/10.1002/aenm.202103564>
- [18] Huidong Xu, Jack Yang, Riyue Ge, Jiujun Zhang, Ying Li, Mingyuan Zhu, Liming Dai, Sean Li, Wenxian Li, Carbon-based bifunctional electrocatalysts for oxygen reduction and oxygen evolution reactions: Optimization strategies and mechanistic analysis, *Journal of Energy Chemistry*, 71, (2022), 234–265 <https://doi.org/10.1016/j.jechem.2022.03.022>
- [19] Yihu Dai, Ye Wang, Bin Liu, Yanhui Yang, Metallic Nanocatalysis: An Accelerating Seamless Integration with Nanotechnology, *Small*, 11, 3, (2015), 268–289 <https://doi.org/10.1002/sml.201400847>
- [20] Rongge Zou, Moriko Qian, Chenxi Wang, Wendy Mateo, Yunpu Wang, Leilei Dai, Xiaona Lin, Yunfeng Zhao, Erguang Huo, Lu Wang, Xuesong Zhang, Xiao Kong, Roger Ruan, Hanwu Lei, Biochar: From by-products of agro-industrial lignocellulosic waste to tailored carbon-based catalysts for biomass thermochemical conversions, *Chemical Engineering Journal*, 441, (2022), 135972 <https://doi.org/10.1016/j.cej.2022.135972>
- [21] David Buceta, Concha Tojo, Miomir B. Vukmirovic, Francis Leonard Deepak, M. Arturo López-Quintela, Controlling Bimetallic Nanostructures by the Microemulsion Method with Subnanometer Resolution Using a Prediction Model, *Langmuir*, 31, 27, (2015), 7435–7439 <https://doi.org/10.1021/acs.langmuir.5b01455>
- [22] Riny Yolanda Parapat, Michael Schwarze, Alwin Ibrahim, Minoo Tasbihi, Reinhard Schomäcker, Efficient preparation of nanocatalysts. Case study: green synthesis of supported Pt nanoparticles by using microemulsions and mangosteen peel extract, *RSC Advances*, 12, 53, (2022), 34346–34358 <https://doi.org/10.1039/D2RA04134K>
- [23] Riny Y. Parapat, Firman A. Yudatama, Maya R. Musadi, Michael Schwarze, Reinhard Schomäcker, Antioxidant as Structure Directing Agent in Nanocatalyst Preparation. Case Study: Catalytic Activity of Supported Pt Nanocatalyst in Levulinic Acid Hydrogenation, *Industrial & Engineering Chemistry Research*, 58, 7, (2019), 2460–2470 <https://doi.org/10.1021/acs.iecr.8b03555>
- [24] Riny Y. Parapat, Veronica Parwoto, Michael Schwarze, Bingsen Zhang, Dang Sheng Su, Reinhard Schomäcker, A new method to synthesize very active and stable supported metal Pt catalysts: thermo-destabilization of microemulsions, *Journal of Materials Chemistry*, 22, 23, (2012), 11605–11614 <https://doi.org/10.1039/C2JM15468D>
- [25] Concha Tojo, David Buceta, Manuel Arturo López-Quintela, On Metal Segregation of Bimetallic Nanocatalysts Prepared by a One-Pot Method in Microemulsions, *Catalysts*, 7, 2, (2017), 68 <https://doi.org/10.3390/catal7020068>
- [26] Mustafa Balat, Mehmet Balat, Elif Kirtay, Havva Balat, Main routes for the thermo-conversion of biomass into fuels and chemicals. Part 1: Pyrolysis systems, *Energy Conversion and Management*, 50, 12, (2009), 3147–3157 <https://doi.org/10.1016/j.enconman.2009.08.014>
- [27] Daegi Kim, Gabin Kim, Doo Young Oh, Kee-Won Seong, Ki Young Park, Enhanced hydrogen production from anaerobically digested sludge using microwave assisted pyrolysis, *Fuel*, 314, (2022), 123091 <https://doi.org/10.1016/j.fuel.2021.123091>
- [28] Oxana N. Fedyaeva, Anatoly A. Vostrikov, Mikhail Ya Sokol, Anna V. Shatrova, Zinc sulfidation by H₂S and H₂S/H₂O supercritical fluids: Synthesis of nanoparticles and catalytic effect of water, *The Journal of Supercritical Fluids*, 95, (2014), 669–676 <https://doi.org/10.1016/j.supflu.2014.09.046>
- [29] Yıldırım İsmail Tosun, Benefaction and Pyrolysis of Sırnak Asphaltite and Lignite, *International Journal of Clean Coal and Energy*, 3, 2, (2014), 13–18 <http://dx.doi.org/10.4236/ijccee.2014.32002>

- [30] Neel Narayan, Ashokkumar Meiyazhagan, Robert Vajtai, Metal Nanoparticles as Green Catalysts, *Materials*, 12, 21, (2019), 3602 <https://doi.org/10.3390/ma12213602>
- [31] Rajender S. Varma, Greener approach to nanomaterials and their sustainable applications, *Current Opinion in Chemical Engineering*, 1, 2, (2012), 123–128 <https://doi.org/10.1016/j.coche.2011.12.002>
- [32] Manh Tung Nguyen, Dang Le Tri Nguyen, Changlei Xia, Thanh Binh Nguyen, Mohammadreza Shokouhimehr, Siva Sankar Sana, Andrews Nirmala Grace, Mortaza Aghbashlo, Meisam Tabatabaei, Christian Sonne, Soo Young Kim, Su Shiung Lam, Quyet Van Le, Recent advances in asphaltene transformation in heavy oil hydroprocessing: Progress, challenges, and future perspectives, *Fuel Processing Technology*, 213, (2021), 106681 <https://doi.org/10.1016/j.fuproc.2020.106681>
- [33] Innocent Chukwunonso Ossai, Aziz Ahmed, Auwalu Hassan, Fauziah Shahul Hamid, Remediation of soil and water contaminated with petroleum hydrocarbon: A review, *Environmental Technology & Innovation*, 17, (2020), 100526 <https://doi.org/10.1016/j.eti.2019.100526>
- [34] Nurullafina Saadah, Susianto Susianto, Ali Altway, Yeni Rachmawati, Catalytic pyrolysis of Asbuton into liquid fuel with Zeolite as catalyst, *Malaysian Journal of Fundamental and Applied Sciences*, 16, 2, (2020), 196–200
- [35] Laibao Zhang, Zhenghong Bao, Shunxiang Xia, Qiang Lu, Keisha B. Walters, Catalytic Pyrolysis of Biomass and Polymer Wastes, *Catalysts*, 8, 12, (2018), 659 <https://doi.org/10.3390/catal8120659>
- [36] Ashley Zachariah, Lin Wang, Shaofeng Yang, Vinay Prasad, Arno de Klerk, Suppression of Coke Formation during Bitumen Pyrolysis, *Energy & Fuels*, 27, 6, (2013), 3061–3070 <https://doi.org/10.1021/ef400314m>
- [37] Ronaldo Irzon, Perbandingan *calorific value* beragam bahan bakar minyak yang dipasarkan di Indonesia menggunakan bomb *calorimeter*, *Jurnal Geologi dan Sumberdaya Mineral*, 22, 4, (2012), 217–223
- [38] Yang Mu, Tingting Wang, Jian Zhang, Changgong Meng, Yifu Zhang, Zongkui Kou, Single-Atom Catalysts: Advances and Challenges in Metal-Support Interactions for Enhanced Electrocatalysis, *Electrochemical Energy Reviews*, 5, (2022), 145–186 <https://doi.org/10.1007/s41918-021-00124-4>
- [39] Dongze Li, Hui Liu, Ligang Feng, A Review on Advanced FeNi-Based Catalysts for Water Splitting Reaction, *Energy & Fuels*, 34, 11, (2020), 13491–13522 <https://doi.org/10.1021/acs.energyfuels.0c03084>
- [40] Riny Y. Parapat, Mulianny Wijaya, Michael Schwarze, Sören Selve, Marc Willinger, Reinhard Schomäcker, Particle shape optimization by changing from an isotropic to an anisotropic nanostructure: preparation of highly active and stable supported Pt catalysts in microemulsions, *Nanoscale*, 5, 2, (2013), 796–805 <https://doi.org/10.1039/C2NR3212J>
- [41] Satish Balasaheb Nimse, Dilipkumar Pal, Free radicals, natural antioxidants, and their reaction mechanisms, *RSC Advances*, 5, 35, (2015), 27986–28006 <https://doi.org/10.1039/C4RA13315C>